Journal of the European Ceramic Society xxx (xxxx) xxx

Contents lists available at ScienceDirect

Journal of the European Ceramic Society

journal homepage: www.elsevier.com/locate/jeurceramsoc

Original Article

Two novel garnet $Sr_3B_2Ge_3O_{12}$ (B = Yb, Ho) microwave dielectric ceramics with low permittivity and high Q

Jie Li [a,b,*], Ying Tang [a,b,*], Zhiwei Zhang [a], Weishuang Fang [a], Laiyuan Ao [a], Aihong Yang [a], Laijun Liu [a], Liang Fang [a,b,*]

[a] Guangxi Key Laboratory of Optical and Electronic Materials and Devices, College of Material Science and Engineering, Guilin University of Technology, Guilin, 541004, China

[b] Key Laboratory of Nonferrous Materials and New Processing Technology, Ministry of Education, Guilin University of Technology, Guilin 541004, China

ARTICLE INFO

Keywords:
Garget structure
Microwave dielectric ceramics
Low permittivity
High
Q value

ABSTRACT

Two cubic garnet-structured $Sr_3B_2Ge_3O_{12}$ (B = Yb, Ho; called SYG and SHG) ceramics synthesised by the high-temperature solid-phase reaction method were investigated in terms of phase formation, sintering behaviour and microwave dielectric performance. At their optimal sintering temperatures, SYG had low dielectric constant (ε_r) = 9.30, high quality factor ($Q \times f$) = 129,360 GHz and negative temperature coefficient of resonant frequency (τ_f) =−42 ppm/℃, whereas SHG exhibited low ε_r = 9.23, $Q \times f$ = 104,600 GHz, and comparatively near-zero τ_f =−26 ppm/℃. The difference in microwave dielectric performance of both ceramics was discussed by the packing fraction, full width at half maximum (FWHM) of A_{1g} Raman mode at 779 cm^{-1} (775 cm^{-1}) and bond valence. The intrinsic dielectric properties of SYG and SHG ceramics were investigated by the infrared reflectivity spectra, and their negative τ_f values were tuned to near-zero.

1. Introduction

Microwave dielectric ceramics have received increasing scientific and commercial attention for their wide application prospects in the 5 G market because of their advantages of small size, light weight and high quality factor ($Q \times f$) [1–4]. The general trend of the working frequency for 5 G communication is millimetre wave, and some special frequency bands are as follows: 24.25–27.5 GHz, 37–43.5 GHz and 66–71 GHz. The primary requirements for millimetre wave application are possessing wide-ranging bandwidth, faster transmission speed with very little time delay and high stability [5–6]. Therefore, new materials with low dielectric constant (ε_r < 20), ultra-low dielectric loss (high Q value >5000 at working frequency) and near-zero τ_f values for thermal stability are required [7–9].

Garnet ceramics $Y_3Al_5O_{12}$ (sintering temperature =1650 °C/24 h, ultrahigh $Q \times f$ = 440,000 GHz, low ε_r = 10.5 and τ_f = -66 ppm/°C) [10] and $Re_3Ga_5O_{12}$ (Re: Nd, Sm, Eu, Dy, Yb and Y) with high sintering temperatures of 1350 °C –1500 °C, high $Q \times f$ (40 000 GHz to 192 173 GHz), low ε_r (11.5–12.5) and a relatively stable τ_f (−33.7 ppm/°C to −12.4 ppm/°C) [11] have been developed with low ε_r and ultralow loss microwave dielectrics are used as microwave resonators and advanced substrates in microwave-integrated circuits. However, their high sintering temperatures impede their practical use. Garnets with a general formula of $A_3B_2C_3O_{12}$ (space group *Ia-3d*, Z = 8) consist of multitype polyhedrons (dodecahedron [A], octahedron [B] and tetrahedron [C]), which have a large variety of compositional derivatives due to the unique crystal structure. Rare earth and alkaline-earth elements generally occupy A sites. B sites mainly accommodate rare-earth and transition-metal elements. Multivalent cations, including V^{5+}/As^{5+} and Si^{4+}/Ge^{4+}, have been reported in C cites [12]. Some vanadate-based garnets exhibited the characteristics of relatively favourable dielectric performance and low sintering temperatures, such as $Sr_2NaMg_2V_3O_{12}$ (ε_r = 11.7, $Q \times f$ = 37,950 GHz and τ_f =−2.9 ppm/°C) [13]; $Na_2PrMg_2V_3O_{12}$ (ε_r = 12.6, $Q \times f$ = 15,040 GHz and τ_f =−45.1 ppm/°C) [14]; $Na_2YbMg_2V_3O_{12}$ (ε_r = 13.1, $Q \times f$ = 22,040 GHz and τ_f =−59.2 ppm/°C) [14]; $Na_2BMg_2V_3O_{12}$ (B = Nd, Sm) with $\varepsilon_r \sim 12$, $Q \times f$ = 26,544 GHz and $\tau_f \sim -69$ ppm/°C [15]; $NaPb_2B_2V_3O_{12}$ (B = Mg, Zn) with $\varepsilon_r \sim 20.6–22.4$, $Q \times f \sim 7{,}900–22{,}800$ GHz, and $\tau_f \sim -6–25.1$ ppm/°C [16]; $AgPb_2B_2V_3O_{12}$ (B = Mg, Zn) with $\varepsilon_r \sim 23.3–26.4$, $Q \times f \sim 26{,}900–28{,}400$ GHz and $\tau_f \sim -18.4–19.3$ ppm/°C [17]. However, these $Q \times f$

* Corresponding authors at: Guangxi Key Laboratory of Optical and Electronic Materials and Devices, College of Material Science and Engineering, Guilin University of Technology, Guilin, 541004, China.

E-mail addresses: jielee2019@aliyun.com (J. Li), tangyinggl001@aliyun.com (Y. Tang), fanglianggl001@aliyun.com (L. Fang).

https://doi.org/10.1016/j.jeurceramsoc.2020.10.018
Received 6 August 2020; Received in revised form 5 October 2020; Accepted 10 October 2020
Available online 15 October 2020

values are ineffective for millimetre wave application. Thus, the search for high Q garnets is still on going.

Recently, some germanate-based garnets reportedly possess relatively high $Q \times f$, such as $Ca_3Al_2GeO_{12}$ ($\varepsilon_r = 7.6$, $Q \times f = 104{,}100$ GHz and $\tau_f = -15$ ppm/°C) [18] and $Ca_3Y_2Ge_3O_{12}$ with the low ε_r of 10.8, high $Q \times f$ value of 97,126 GHz and τ_f value of −40.6 ppm/°C) [19]. Fang et al. revealed the influence of diverse cation distributions at A site on the properties of garnet-structure microwave dielectric ceramics [19]. $Sr_3B_2Ge_3O_{12}$ (B = Yb, Ho) belonging to the garnet family, have been investigated as good host lattice materials for luminescent properties [20,21]. The effect of different cations in B site in $Sr_3B_2Ge_3O_{12}$ garnet ceramics on dielectric performance has not been studied. Thus, in this study, garnet-structure ceramics $Sr_3B_2Ge_3O_{12}$ (B = Yb, Ho) were prepared, and their phase evolution, microstructure and microwave dielectric properties were explored. Raman spectra and infrared reflectivity spectra were analysed to study the relationship between intrinsic dielectric performance and crystal structure.

2. Experimental procedures

The $Sr_3B_2Ge_3O_{12}$ (B = Yb, Ho) ceramics were fabricated via a high-temperature solid-state method by using high-purity $SrCO_3$, Yb_2O_3, Ho_2O_3 and GeO_2 as raw materials. The $Sr_3B_2Ge_3O_{12}$ powders were weighed and ground thoroughly for 4 h, dried, and then calcined at 1100 °C for 6 h. After remilling, they were pressed into cylinders of 10 mm × 6.5 mm size using 5 wt.% PVA as binder. The pellets were initially heated at 550 °C for 2 h to eliminate organic binder, and then sintered at 1200 °C – 1280 °C for 6 h.

Panalytical X'Pert PRO diffractometer was used to analyse the phase composition and crystal structure of ceramics. The phase formation was analysed by a simultaneous thermal instrument (STA449F3). The microstructures of the polished and thermally etched surface of the samples were observed by S4800 scanning electron microscope (Hitachi, Tokyo, Japan) equipped with energy dispersive spectrometer (EDS). The ceramics were polished using Phoenix 4000 sample preparation system. The polished samples were thermally etched at 50 °C below sintering temperature for 35 min. The average grain size was determined using the linear intercept [22]. Raman measurements were performed by Thermo Fisher Scientific DXR with 532 nm line of the Nd: YAG laser beam. The spectra were measured from 100 cm^{-1} to 1000 cm^{-1} with the spectral resolution prior to 1 cm^{-1}. The bulk densities of ceramics were tested using Archimedes method. The microwave dielectric performance (ε_r, $Q \times f$ and τ_f) was analysed by a network analyser (N5230A, Agilent) with a temperature chamber. The τ_f values were measured in the temperature range of 25 °C to 85 °C. Infrared reflectivity spectra were conducted using a Bruker IFS 66v Fourier transform infrared spectrometer (NSRL, China) at 50 cm^{-1} to 1000 cm^{-1} at room temperature with the spectral resolution of 0.25 cm^{-1}.

3. Results and discussion

To ascertain the formation of garnet phase SYG and SHG, TG/DSC analyses of both raw mixtures were conducted at 25 °C – 1200 °C (Fig. 1). The TG bight of the mixtures of $SrCO_3$, Yb_2O_3 and GeO_2 exhibits only a weak mass loss during 25 °C – 700 °C caused by the loss of H_2O or carbon dioxide. $SrCO_3$ undergoes a phase change from the orthogonal phase to triangular high-temperature modification at 913 ℃ prior to decomposition [23]. At approximately 1100 °C, the endothermic peak of strontium carbonate decomposition occurs. In addition, the exothermic formation of garnet SYG is initiated, and this process is completed at 1158 °C. The various trend in TG/DSC curves of SHG raw mixtures is analogous with that of SYG, and the garnet formation for SHG is finalised at 1150 °C.

X-ray powder diffraction analyses of both samples sintered at different temperatures were conducted to confirm the phase-formation temperatures (Fig. S1). When sintering at 1050 °C and 1075 °C, the X-ray diffraction (XRD) curves show that mixed phases exist in SYG and SHG ceramics, comprising SYG/SHG, Sr_2GeO_4, $SrGeO_3$ and Yb_2O_3/Ho_2O_3 phases. When the sintering temperatures exceed 1100 °C, only the diffraction peaks of SYG (JCPDS#29-1319) or SHG (JCPDS#29-1302) are observed. This finding indicates that the garnet formation of SYG and SHG evidently occurs at 1100 °C, consistent with thermal analysis.

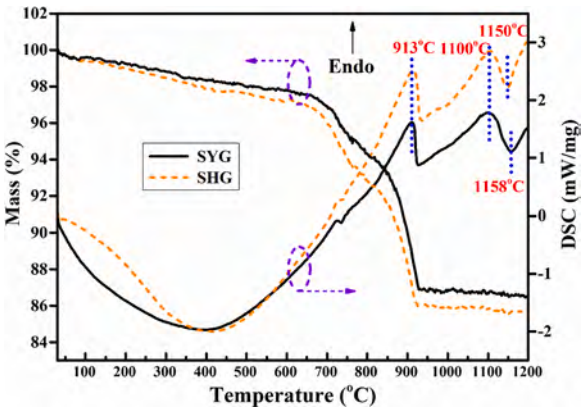

Fig. 1. TG/DSC curves of a powder blend out of stochiometric amounts of SYG and SHG.

Fig. 2a illustrates the XRD patterns of SYG and SHG ceramics sintered at 1240 °C and 1260 °C, respectively. The figure shows that all diffraction patterns can be indexed to a standard cubic garnet SYG and SHG phases with a space group of *Ia-3d* ($Z = 8$), and that no secondary phase is detected. Table S1 lists the refined Wyckoff positions, occupancy, atomic coordinates and atomic displacement parameters of SYG and SHG ceramics. Fig. 2b–c show the profile fits for the Rietveld refinement of SYG and SHG ceramics. The lattice parameters are calculated as a =13.0273 Å, V = 2210.8752 $Å^3$ and a =13.0942 Å, V = 2245.1268 $Å^3$, and the Rietveld discrepancy factors R_p (%) and R_{wp}(%) are 5.24% (5.73%) and 6.81% (7.66%), respectively. Evidently, the unit cell volume of SHG is larger than that of SYG due to the larger ionic radius of Ho^{3+} (0.901 Å, coordination number CN = 6) than Yb^{3+} (0.868 Å, coordination number CN = 6). The refined bond length and bond valence are listed in Table 1. In the structure (Fig. 2d), Sr^{2+} occupies the 24*c* position, with eight oxygen atoms of dodecahedron. The position 16*a* at the centre of the oxygen octahedron is occupied by Yb^{3+}/Ho^{3+}. Ge^{4+} occupies the 24*d* position at the centre of the oxygen tetrahedra. Oxygen atoms are in the general position 96*h*.

The microscopic morphology examination of the polished and thermally etched surfaces of SYG and SHG ceramics sintered at their optimum temperatures is shown in Fig. 3. Both ceramics show a dense and homogeneous structure and recognisable grain boundaries. SYG has smaller and uniform polygonal grains (average size ~ 1.25 μm), whereas SHG exhibits a larger grain size (average size ~ 3.50 μm).

Fig. 4 illustrates the variations in relative density and microwave dielectric properties (ε_r, $Q \times f$ and τ_f) of both ceramics sintered at various temperatures. As shown in Fig. 4(a), with the increment in temperature, the relative density rapidly increases, reaching the maximum values of 96.7 % at 1240 ℃for SYG and 96.2% at 1260 ℃ for SHG, and then marginally decreases. ε_r and $Q \times f$ values exhibit a similar trend to relative density with sintering temperature. The SYG ceramic sintered at 1240 °C possesses optimal comprehensive performance with low ε_r = 9.30, high $Q \times f$ = 129,360 GHz and negative τ_f =−42 ppm/℃. SHG ceramic sintered at 1260 ℃ exhibits a low ε_r = 9.23, $Q \times f$ = 104,600 GHz and relatively near-zero τ_f =−26 ppm/℃. The difference in $Q \times f$ and τ_f values of both ceramics is discussed on account of crystal structure detailly in the following section.

Non-intrinsic (impurity, grain boundary, relative density or pores) and intrinsic factors (crystal structure) affect dielectric performance in

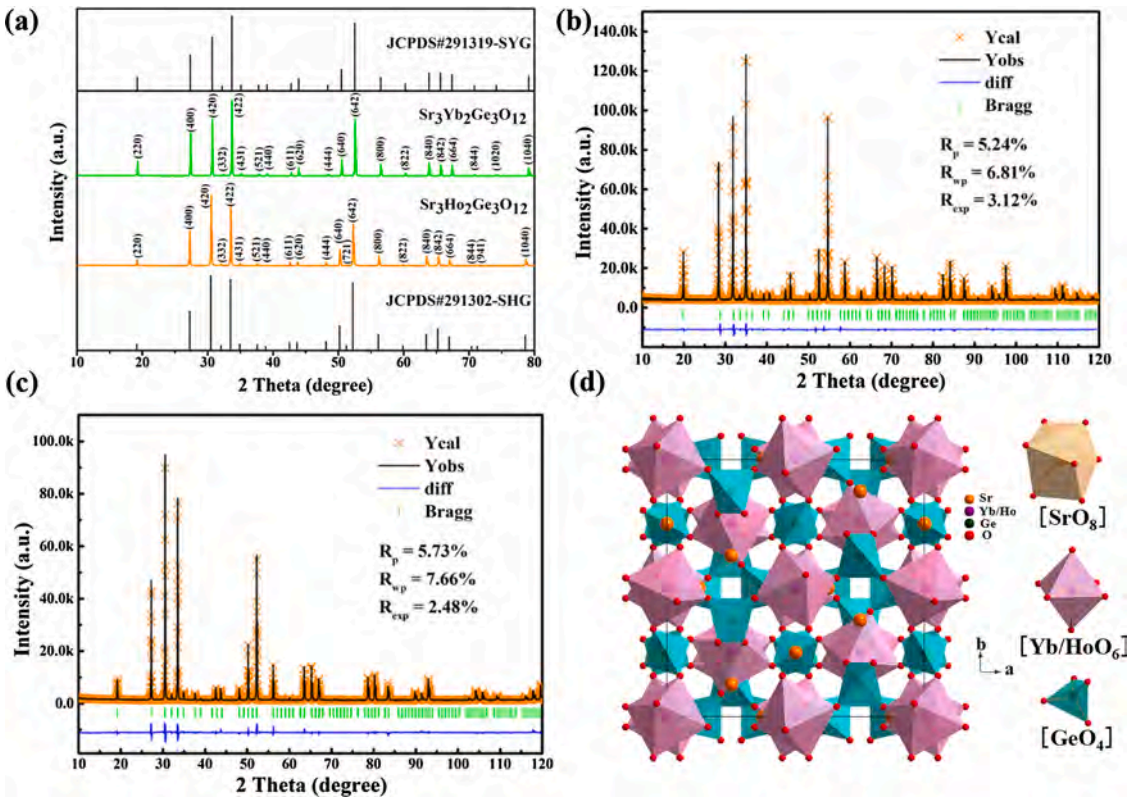

Fig. 2. (a) XRD patterns and Rietveld refinement plots of SYG (b) and SHG (c) ceramic sintered 1240 °C and 1260 °C, respectively; (d) the schematic crystal structure of both ceramics.

Table 1
The bond valence of $Sr_3B_2Ge_3O_{12}$ (B = Yb, Ho).

Samples	R_{Sr}(Å)	R_B(Å)	$d_{Sr\text{-}O}$(Å)	$d_{B\text{-}O}$(Å)	b(Å)	V_{Sr}	V_B
SYG	2.118	1.985	2.6593	2.2840	0.37	1.86	2.67
SHG	2.118	2.023	2.6408	2.2415	0.37	1.94	3.32

the microwave range. The extrinsic factors can be neglected for samples sintered at the optimal temperature because of the single phase and dense and isotropous grains. Here, the theoretical dielectric constant (ε_{th}) is calculated using Clausius–Mossotti formula, as follows [24,25]:

$$\varepsilon_{th} = \frac{3V + 8\pi\alpha}{3V - 4\pi\alpha} \quad (1)$$

where V and α are the cell volume and the total molecular polarisability, respectively. Accordingly, ε_{th} of SYG and SHG is 9.60 and 9.58, respectively. ε_r could be amended by Bosman and Having's formula to eliminate the effect of porosity, as follows:

$$\varepsilon_{corr} = \varepsilon_r(1 + 1.5p)\varepsilon_{corr} = \varepsilon_r(1 + 1.5\,p) \quad (2)$$

where p refers to the fractional porosity. ε_{corr} values of SYG at 1240 °C and SHG at 1260 °C are 9.76 and 9.75, respectively. The slight deviation between ε_{corr} and ε_{th} for CYG and MYG signifies that the ionic polarisation is responsible for the dielectric response in the microwave range. Notably, the measured bond valence of Sr^{2+} in A site for SYG and SHG is 1.86 and 1.94, respectively. These values slightly offset with the theoretical bond valence of 2 for Sr^{2+}, thereby resulting in stable SYG and SHG garnet compounds (Table 1). Therefore, the measured ε_r in SYG and SHG ceramics is relatively close to the ε_{th} values; it is relatively different from that in the garnet MYG due to the abnormally small bond valence of 1.25 for Mg^{2+} at A site [19].

Kim et al. reported that the $Q \times f$ value is positively associated with

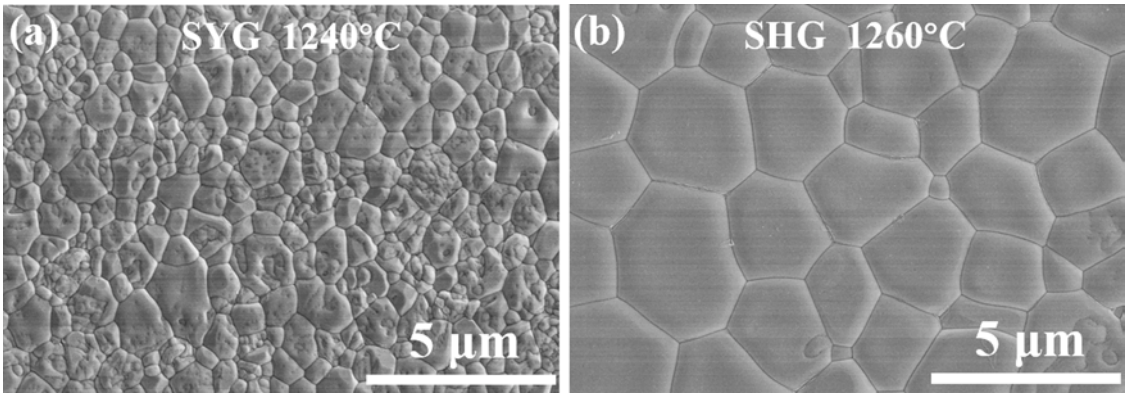

Fig. 3. The SEM images of the polished and thermally etched surfaces of SYG and SHG ceramics sintered at their optimum temperatures.

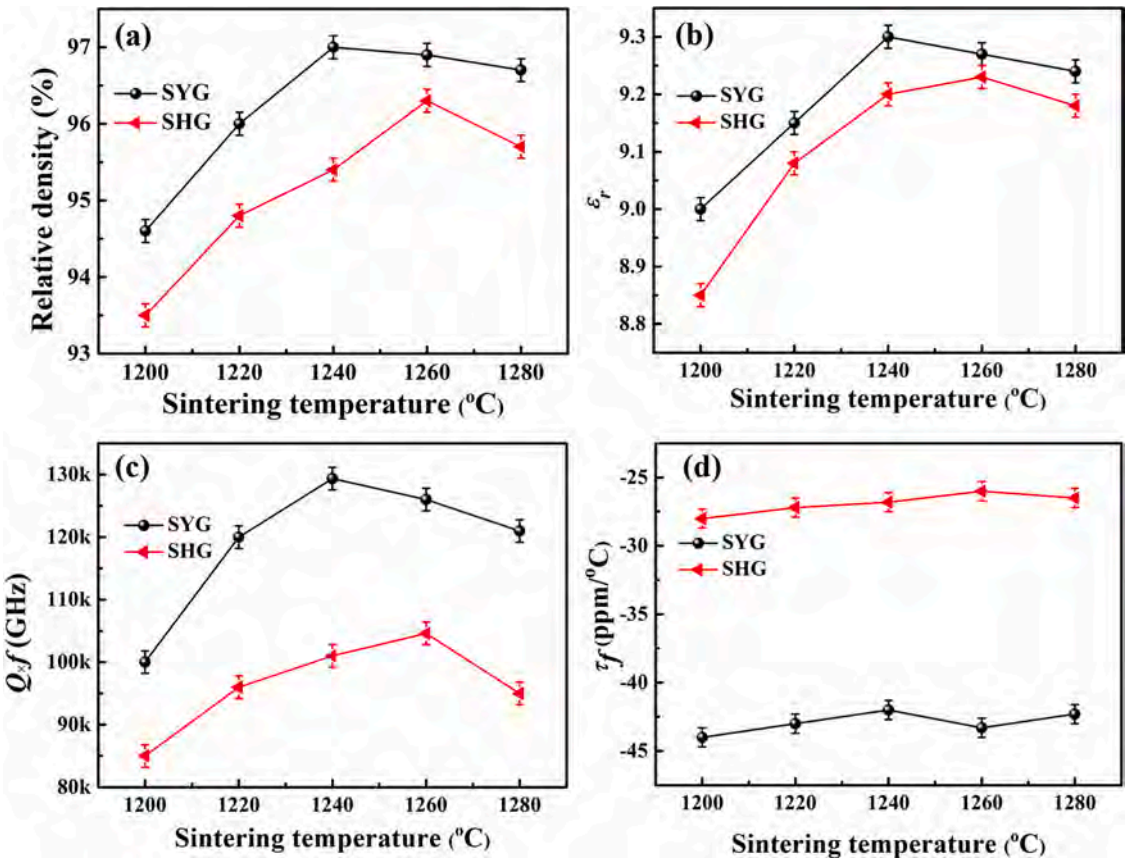

Fig. 4. The variations in relative density and microwave dielectric properties of both ceramics as a function of sintering temperature.

the packing fraction calculated by equation (2), as follows [26]:

$$\text{packing fraction } (\%) = \frac{Volume\ of\ packing\ ions}{Volume\ of\ unit\ cell} Z \quad (3)$$

Table S2 lists the microwave dielectric performance and packing fraction of SYG and SHG ceramics. The packing fraction of SYG (59.14 %) is lower than that of SHG (58.47 %). The increase in packing fraction can reduce the vibration of the crystal lattice and thus enhance the quality factor ($Q \times f = 129{,}360$ GHz for SYG, $Q \times f = 104{,}600$ GHz for SHG) [27]. Bond valence is a significant parameter appertained to the τ_f values. As shown in Table 1, the bond valence of Yb-O in B-site for SYG (2.67) is lower than that of Ho-O for SHG (3.32). Glazer demonstrated the bond valence theory [28], indicating that as the bond valence decreases, the bond energy required to restore the deformation of oxygen polyhedral decreases, and ultimately the $|\tau_f|$ increases. Therefore, the larger $|\tau_f|$ value of SYG might be related to the decreased bond valence.

Raman spectrum is an effective tool to study the lattice vibration information, whose variation causes changes in Raman shift and Raman full width at half maximum (FWHM). The Raman spectra and the Gaussia-Lorentzian modes of SYG and SHG ceramics are shown in Fig. 5. On the basis of group theory analysis, 25 Raman active modes for garnets with *Ia*-3*d* space group are estimated, as follows: $\Gamma_{Raman} = 3A_{1g} + 8E_g + 14T_{2g}$. The number of the observed modes fitting by the Gauss-Lorentz function is evidently less than the predicted modes due to the influence of cross coverage of peaks or low resolution of the apparatus. According to the reports, the highest peaks at 779 and 775 cm^{-1} for SYG and SHG, respectively, are attributed to the symmetric stretching mode (A_{1g} Raman mode) of GeO_4 tetrahedron, which can reflect the structure

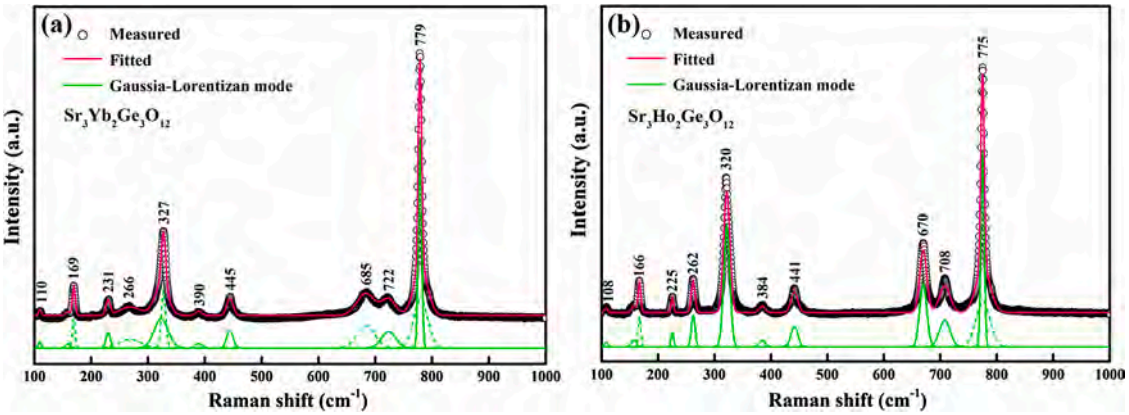

Fig. 5. Raman spectra of SYG and SHG ceramics.

characteristics to dielectric performance [29,30]. Compared with SYG, the Raman modes of SHY exhibit a red shift and a narrower FWHM. The red shift is associated with the larger bond distance and lattice volume of SHY than that of SYG. In general, with the decrease in FWHM, the space of lattice vibration and the nonharmonic vibration decrease, thereby resulting in the decrease in inherent dielectric loss [31]. Therefore, SYG has a narrower FWHM and lower dielectric loss than that of SHG. A similar inverse relation between $Q\times f$ and FWHM of lattice vibration modes is reported in $AgPb_2B_2V_3O_{12}$ (B = Mg, Zn) and $A_3Y_2Ge_3O_{12}$ (A = Ca, Mg) ceramics [17,19]. Table S2 lists the FWHM of the A_{1g} mode for SYG and SHG ceramics.

To understand the inherent dielectric performance of SYG and SHG ceramics deeply, the experimental and fitted IR reflectivity spectra are shown in Fig. 6; they are analysed by the classical harmonic oscillator model as follows [32]:

$$\varepsilon^*(\omega) = \varepsilon_\infty + \sum_{j=1}^{n} \frac{\omega_{pj}^2}{\omega_{oj}^2 - \omega^2 - j\gamma_j\omega} \tag{4}$$

The related terms in the above formula are described in detail in the literature [33]. The relationship between complex reflectivity $R(\omega)$ and permittivity can be expressed as follows:

$$R(\omega) = \left|\frac{1-\sqrt{\varepsilon^*(\omega)}}{1+\sqrt{\varepsilon^*(\omega)}}\right|^2 \tag{5}$$

The infrared reflection spectra of SYG and SHG ceramics can be well fitted with 16 modes. Table S3 lists the relevant phonon parameters of SYG ceramic as representative data. As the XRD results discussed above, the space group of SYG and SHG ceramics is *Ia*-3*d* (No. 230), which has $17T_{1u}$ infrared active modes based on the prediction of group theory. Thus, the number of fitted modes is less than the theoretical modes. The fitted infrared reflection spectra and the complex dielectric constants indicate that the calculated permittivity values for SYG and SHG are 9.02 and 9.01, respectively, and the calculated $Q\times f$ values for SYG and SHG are 143,761 and 121,604 GHz, respectively. Moreover, the calculated dielectric constant and dielectric loss values are close to the measured values (using the $TE_{01\delta}$ method). This finding indicates that the phonon absorption in the infrared region mainly contributes to dielectric polarisation in the microwave band.

Table 2 summarises the sintering temperature, resonant frequency and microwave dielectric properties of Ge-based compounds with garnet structure. By comparison, all the listed Ge based garnets possess low permittivity (~10), high $Q\times f$ values and largely negative τ_f values except for $Mg_3Y_2Ge_3O_{12}$ due to the 'rattling' Mg^{2+} and Y^{+3} in the A site. Notably, the sintering temperatures of SYG and SHG are lower than the other Ge-based garnets, and the τ_f value of SHG is closer to zero than that of the other Ge-based garnets, which is beneficial to practical applications.

Table 2
Sintering temperature and microwave dielectric properties of Ge based compounds with garnet structure

Sample	S.T. (℃)	ε_r	$Q\times f$ (GHz)	f (GHz)	τ_f (ppm/℃)	Ref
$Ca_3Y_2Ge_3O_{12}$	1340	10.80	97,126	13.2	–40.6	[19]
$Mg_3Y_2Ge_3O_{12}$	1460	14.10	12,600	11.5	+120.5	[19]
$Ca_4ZrGe_3O_{12}$	1340	10.68	76,900	-	–41.3	[34]
$Ca_3Al_2Ge_3O_{12}$	1340	8.97	114,871	14.017	–54.6	[35]
$Ca_3Ga_2Ge_3O_{12}$	1320	9.79	129,356	14.293	–50.19	[35]
SYG	1240	9.30 ± 0.1	129,360 ± 600	15.44	−42 ± 1.2	This work
SHG	1260	9.23 ± 0.1	104,600 ± 500	15.75	−26 ± 1.0	This work

The microwave dielectrics demand a near-zero τ_f to satisfy the thermal stability of electronic devices. In this work, $CaTiO_3$ was added to adjust τ_f by forming composite ceramics. Fig. 7a presents that only the diffraction peaks of SYG/SHG and $CaTiO_3$ are observed in 0.95SYG-0.05$CaTiO_3$ and 0.96SHG-0.04$CaTiO_3$ ceramics. The BSE image analysis result indicates that the grains of two different grey scales are clearly shown, and the marked darker grains belong to $CaTiO_3$. The microwave dielectric performance of (1-*x*)SYG-*x*$CaTiO_3$ and (1-*x*)SHG-*x*$CaTiO_3$ ceramics is listed in Table 3. Near-zero τ_f values of +2.7 ppm/℃ and +3.3 ppm/℃ are obtained in 0.95SYG-0.05$CaTiO_3$ and 0.96SHG-0.04$CaTiO_3$ ceramics, respectively.

4. Conclusions

In this study, cubic garnet-structured SYG and SHG ceramics were synthesised at 1100 ℃–1280 ℃ by conventional solid-phase reaction method. Dense and homogeneous ceramics were obtained at 1240 ℃ for SYG with low $\varepsilon_r = 9.30$, high $Q\times f = 129{,}360$ GHz and negative $\tau_f = -42$ ppm/℃. In addition, while SHG ceramics sintered at 1260 ℃ exhibited low $\varepsilon_r = 9.23$, $Q\times f = 104{,}600$ GHz and relatively near-zero τ_f of −26 ppm/℃. The measured ε_r in SYG and SHG ceramics was relatively close to the theoretical ε_{th} values. The difference in $Q\times f$ values was highly dependent on the packing fraction and FWHM of A_{1g} Raman mode at 779 cm^{-1} (775 cm^{-1}). The larger $|\tau_f|$ value of SYG was related to the decreased bond valence. In the microwave band, the dielectric polarisation primarily resulted from the phonon absorption in the infrared region. The negative τ_f values of SYG and SHG ceramics were tuned to near-zero by forming composite ceramics with $CaTiO_3$.

Declaration of Competing Interest

The authors declare that they have no known competing financial interests or personal relationships that could have appeared to influence

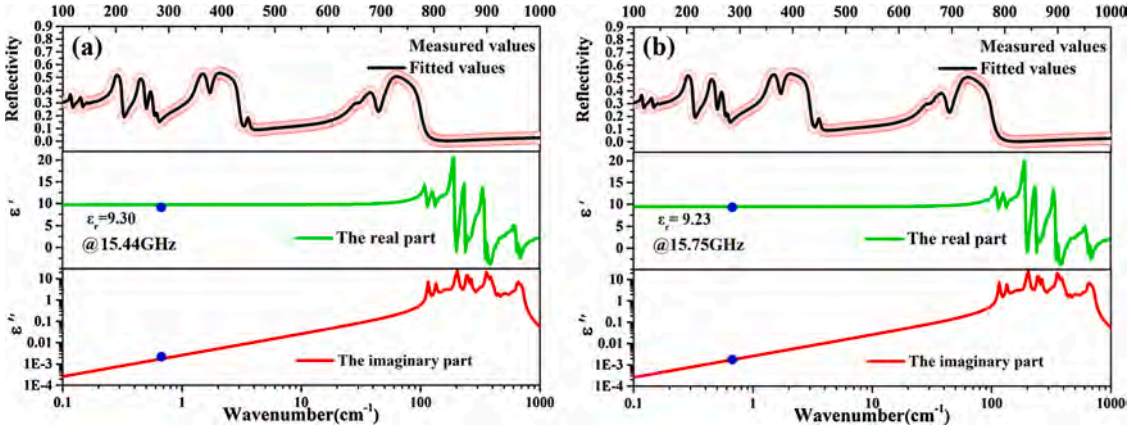

Fig. 6. The measured, fitted IR spectra, and fitted complex dielectric response for SYG (a) and SHG (b) ceramics.

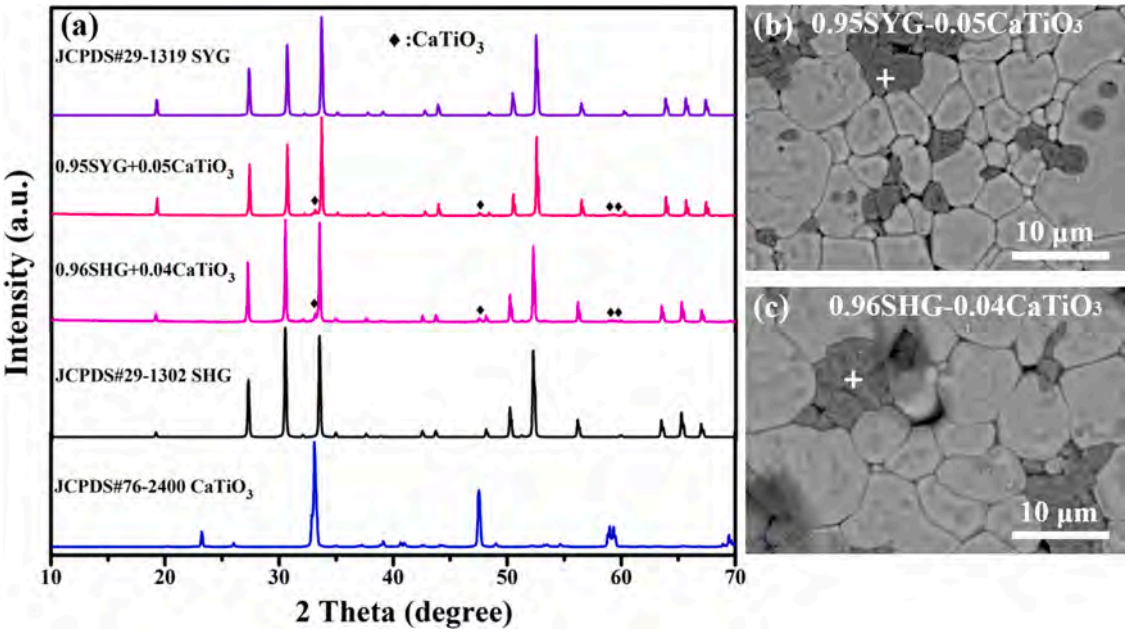

Fig. 7. The XRD and BSE images of 0.95SYG-0.05$CaTiO_3$ and 0.96SHG-0.04$CaTiO_3$ ceramics.

Table 3
Microwave dielectric properties of (1-*x*)SYG-*x*$CaTiO_3$ and (1-*x*)SHG-*x*$CaTiO_3$ceramics

Composition	*x* values	S.T. (℃)	ε_r	$Q \times f$ (GHz)	τ_f (ppm/°C)
SYG	0	1240	9.30 ± 0.1	129,360 ± 600	−42 ± 1.2
	0.03	1240	10.0 ± 0.1	118,673 ± 450	−15.5 ± 1.0
	0.05	1260	10.8 ± 0.1	112,632 ± 500	+2.7 ± 1.2
	0.07	1260	11.4 ± 0.1	108,120 ± 550	+16.8 ± 1.1
SHG	0	1260	9.23 ± 0.1	104,600 ± 500	−26 ± 1.0
	0.02	1260	9.8 ± 0.1	90,136 ± 450	−10.1 ± 1.1
	0.04	1280	10.4 ± 0.1	87,304 ± 600	+3.3 ± 1.2
	0.06	1280	11.0 ± 0.1	82,438 ± 500	+20.4 ± 1.0

the work reported in this paper.

Acknowledgments

This work was supported by Natural Science Foundation of China (Nos. 21761008 and 21965009), the Natural Science Foundation of Guangxi Zhuang Autonomous Region (Nos. 2018GXNSFAA138175) and the Supported by Foundation of Guilin University of Technology (GUTQDJJ2019183).

References

[1] H.H. Guo, D. Zhou, C. Du, P.J. Wang, W.F. Liu, L.X. Pang, Q.P. Wang, J.Z. Su, C. Singh, S. Trukhanov, Temperature stable $Li_2Ti_{0.75}(Mg_{1/3}Nb_{2/3})_{0.25}O_3$-based microwave dielectric ceramics with low sintering temperature and ultra-low dielectric loss for dielectric resonator antenna applications, J. Mater. Chem. C. 8 (2020) 4690–4700.
[2] K. Xiao, L. Gong, M. Kadoch, Opportunistic multicast NOMA with security concerns in a 5G massive MIMO system, IEEE Commun. Mag. 56 (2018) 91–95.
[3] M.B. Krishna, M.J. Lloret, Advances in mobile computing and communications: perspectives and emerging trends in 5G networks, CRC Press, Boca Raton, 2016.
[4] Y.H. Jung, J. Lee, Y. Qiu, N. Cho, S.J. Cho, H.L. Zhang, S. Lee, T.J. Kim, S. Gong, Z. Q. Ma, Stretchable twisted-pair transmission lines for microwave frequency wearable electronics, Adv. Funct. Mater. 26 (2016) 4635–4642.
[5] X.K. Lan, J. Li, J.P. Li, F. Wang, W.Z. Lu, X.C. Wang, W. Lei, Phase evolution and microwave dielectric properties of novel $LiAl_{5-x}Zn_xO_{8-0.5x}$-based ($0 \le x \le 0.5$) ceramics, Ceram. Inter. 103 (2020) 1105–1112.
[6] K. Du, J. Fan, Z.Y. Zou, X.Q. Song, W.Z. Lu, W. Lei, Crystal structure, phase compositions, and microwave dielectric properties of malayaite-type $Ca_{1-x}Sr_xSnSiO_5$ ceramics, J. Am. Ceram. Soc. (2020) 1–9, https://doi.org/10.1111/jace.17360.
[7] Y.B. Chen, C.L. Huang, S.T. Tasi, New dielectric material system of $x(Mg_{0.95}Zn_{0.05}Ti)O_3$-(1-$x$)$Ca_{0.8}Sm_{0.4/3}TiO_3$ at microwave frequency, Mater. Lett. 62 (2008) 2454–2457.
[8] H. Li, B. Tang, X. Li, Z. Qing, Y. Li, H. Yang, Q. Wang, S. Zhang, The structure and properties of 0.95$MgTiO_3$-0.05$CaTiO_3$ ceramics doped with Co_2O_3, J. Mater. Sci. 49 (2014) 5850–5855.
[9] X.J. Yang, S.H. Ding, X.B. Liu, B. Yu, X.L. Yang, T.X. Song, The structure and properties of 0.95$MgTiO_3$-0.05$CaTiO_3$ ceramics co-doped with ZnO–ZrO_2, Ceram. Inter. 38 (2012) S61–S64.
[10] I. Kagomiya, Y. Matsuda, K. Kakimoto, H. Oshato, Microwave dielectric properties of YAG ceramics, Ferroelectrics 387 (2009) 1–6.
[11] J.C. Kim, M.H. Kim, J.B. Lim, S. Nahm, Synthesis and microwave dielectric properties of $Re_3Ga_5O_{12}$ (Re: Nd, Sm, Eu, Dy, Yb, and Y) ceramics, J. Am. Ceram. Soc. 90 (2007) 641–644.
[12] Z. Song, D.D. Zhou, Q.L. Liu, Tolerance factor and phase stability of the garnet structure, Acta Crystallogr. C 75 (2019) 1353–1358.
[13] H.C. Xiang, L. Fang, X.W. Jiang, T. Ying, C.C. Li, A novel temperature stable microwave dielectric ceramic with garnet structure: $Sr_2NaMg_2V_3O_{12}$, J. Am. Ceram. Soc. 99 (2016) 399–401.
[14] M.Y. Xu, H.C. Xiang, L. Fang, Y. Tang, C.C. Li, Two low-firing microwave dielectric ceramics $Na_2LnMg_2V_3O_{12}$ (Ln=Pr, Yb) and their chemical compatibility with silver, J. Mater. Sci-Mater. Electron. 28 (2017) 12342–12347.
[15] Y. Tang, X.W. Jiang, H.C. Xiang, C.C. Li, L. Fang, X.R. Xing, Two novel low-firing $Na_2AMg_2V_3O_{12}$ (A=Nd, Sm) ceramics and their chemical compatibility with silver, Ceram. Inter. 43 (2017) 2892–2898.
[16] M. Rakhi, G. Subodh, Crystal structure and microwave dielectric properties of $NaPb_2B_2V_3O_{12}$ (B=Mg, Zn) ceramics, J. Eur. Ceram. Soc. 38 (2018) 4962–4966.
[17] M. Rakhi, G. Subodh, Crystal structure, phonon modes, and bond characteristics of $AgPb_2B_2V_3O_{12}$ (B = Mg, Zn) microwave ceramics, J Am Ceram Soc. 103 (2020) 3157–3167.
[18] H.F. Zhou, C.M. Lu, S.X. Li, J.J. Deng, K.G. Wang, Phase composition, sintering behavior and microwave dielectric properties of novel high Q Ca3Al2(GeO4)3 ceramic Mater. Lett. (263)2020 127240.
[19] Y. Tang, Z.W. Zhang, J. Li, M.Y. Xu, Y.F. Zhai, L. Duan, C.X. Su, L.J. Liu, Y.H. Sun, L. Fang, $A_3Y_2Ge_3O_{12}$ (A=Ca, Mg): Two novel microwave dielectric ceramics with contrasting τ_f and $Q \times f$, J. Eur. Ceram. Soc. 40 (2020) 3989–3995.
[20] S.K. Hussain, L.K. Bharat, D.H. Kim, J.S. Yu, Facile pechini synthesis of $Sr_3Y_2Ge_3O_{12}$: Bi^{3+}/Eu^{3+} phosphors with tunable emissions and energy transfer for WLEDs, J. Alloys. Compd. 703 (2017) 361–369.
[21] D. Pasiński, E. Zych, J. Sokolnicki, Relationship between structure and luminescence properties in Ce^{3+} or Ce^{3+}, Mn^{2+} -doped garnet phosphors for use in white LEDs, J. Lumin. 169 (2016) 862–867.

[22] M.I. Mendelson, Average grain size in polycrystalline ceramics, J. Am. Chem. Soc. 52 (1969) 443–446.
[23] D. Uhlich, J. Plewa, T. Jüstel, Phase formation and characterization of $Sr_3Y_2Ge_3O_{12}$, $Sr_3In_2Ge_3O_{12}$, and $Ca_3Ga_2Ge_3O_{12}$ doped by trivalent europium, J. Lumin. 128 (2018) 1649–1654.
[24] R.D. Shannon, Dielectric polarizabilities of ions in oxides and fluorides, J. Appl. Phys. 73 (1993) 348–366.
[25] S.H. Yoon, D.W. Kim, S.Y. Cho, K.S. Hong, Investigation of the relations between structure and microwave dielectric properties of divalent metal tungstate compounds, J. Eur. Ceram. Soc. 26 (2006) 2051–2054.
[26] E.S. Kim, B.S. Chun, R. Freer, R.J. Cernik, Effects of packing fraction and bond valence on microwave dielectric properties of $A^{2+}B^{6+}O_4$ (A^{2+}: Ca, Pb, Ba; B^{6+}: Mo, W) ceramics, J. Eur. Ceram. Soc. 30 (2010) 1731–1736.
[27] C.C. Li, H.C. Xiang, Y. Tang, M.Y. Xu, J. Khaliq, J.Q. Chen, L. Fang, Low-firing and temperature stable microwave dielectric ceramics: $Ba_2LnV_3O_{11}$ (Ln=Nd, Sm), J. Am. Ceram. Soc. 101 (2018) 773–781.
[28] A.M. Glazer, The classification of tilted octahedral perovskites, Acta Crys-tallogr. B28 (1972) 3384–3392.
[29] J.A. Koningstein, O.S. Mortensen, Laser-excited phonon Raman spectrum of garnets, J. Mol. Spectrosc. 27 (1968) 343–350.
[30] W.B. White, V.G. Keramidas, Raman spectra of yttrium iron garnet and two vanadium garnets, J. Am. Ceram. Soc. 54 (1971) 472–483.
[31] Z.F. Fu, P. Liu, J.L. Ma, X. Zhao, H. Zhang, Novel series of ultra-low loss microwave dielectric ceramics: $Li_2Mg_3BO_6$ (B=Ti, Sn, Zr), J. Eur. Ceram. Soc. 36 (2016) 625–629.
[32] C. Xing, J.Z. Li, J. Wang, H.L. Chen, H.Y. Qiao, X.Q. Yin, Q. Wang, Z.M. Qi, F. Shi, Internal Relations between Crystal Structures and Intrinsic Properties of Nonstoichiometric $Ba_{1+x}MoO_4$ Ceramics, Inorg. Chem. 57 (2018) 7121–7128.
[33] H.H. Guo, D. Zhou, L.X. Pan, Z.M. Qi, Microwave dielectric properties of low firing temperature stable scheelite structured $(Ca,Bi)(Mo,V)O_4$ solid solution ceramics for LTCC applications, J. Eur. Ceram. Soc. 39 (2019) 2365–2373.
[34] C.X. Su, L.Y. Ao, Y.F. Zhai, Z.W. Zhang, Y. Tang, J.Q. Chen, L.J. Liu, L. Fang, Novel low-permittivity microwave dielectric ceramics in garnet-type $Ca_4ZrGe_3O_{12}$, Mater. Lett. 275 (2020) 128149.
[35] Y.F. Zhai, Y. Tang, J. Li, L. Duan, C.X. Su, A.L. Cao, C.Y. Jin, L. Fang, Structure, Raman spectra and properties of two low-ε_r microwave dielectric ceramics $Ca_3B_2Ge_3O_{12}$ (B = Al, Ga), Ceram. Int. (2020), https://doi.org/10.1016/j.ceramint.2020.08.031.